Journal of Manufacturing Engineering, September 2014, Vol. 9, Issue. 3, pp 143-148

EFFECT OF IMMERSION TIME ON THE CORROSION BEHAVIOR OF FRICTION STIR WELDED AA2024 ALUMINIUM ALLOY WELDS

[*]Seetharaman R[1], Ravisankar V[2] and Balasubramanian V[3]

[1]Assistant Professor, Department of Manufacturing Engineering, Annamalai University, Chidambaram – 608 002, Tamil nadu, INDIA
[2 & 3]Professor, Department of Manufacturing Engineering, Annamalai University, Chidambaram – 608 002, Tamil nadu, INDIA.

ABSTRACT

In this research, the corrosion behaviour of friction stir welded AA2024 aluminium alloy immersed in NaCl solution with different immersion times have been investigated using immersion corrosion tests. The microstructural characterization was examined using light optical microscopy and scanning electron microscopy. It is resulted that with the increase of immersion time, the corrosion rate decreases for the specimens undergoing immersion corrosion tests. It proved that the outer layer made a predominant role to strike against corrosion with the increase of time. The decrease in both corrosion pit area and depth, the increase of time is caused by general corrosion reducing the area surrounding the pits, as well as reducing the pit depth simultaneously. General corrosion removes the surrounding aluminium, thereby shrinking some pits and reducing their volume. Thus with the increase of immersion time the corrosion rate decreases.

Keywords: *AA2024 Aluminium alloy, Friction stir welding, Immersion corrosion test.*

1. Introduction

Aluminum alloys are widely used in the aeronautical industry and marine engineering due to their light mass and advantageous mechanical properties. However, these alloys have a low resistance against corrosion because of the presence of alloying elements which can locally break down the passive film and allow the attack of aggressive ions like chloride ions that can initiate pitting or crevice corrosion [1]. Friction stir welding (FSW), a new solid state joining technique, was invented by The Welding Institute (TWI) in 1991 [2]. This technique is now increasingly used to join high strength aluminium alloys (2xxx, 6xxx, 7xxx and 8xxx series) for aerospace, automotive and marine applications [3]. This technique is attractive for joining high strength aluminium alloys since there is far lower heat input during the process compared with conventional welding methods such as TIG or MIG. This solid state process leads to minimal microstructural changes and better mechanical properties than conventional welding [4, 5].

In the welding field, extensive research on friction stir welded joints for AA2000 or AA7000 series aluminium alloys have been carried out in the past decade focusing on microstructural characteristics, mechanical properties, residual stress analysis, plastic flow patterns and numerical simulation for the temperature field [6-7] . However, there are only a few investigations related to the corrosion properties of the FSW aluminium alloys.

The electrochemical behaviour of aluminum and its alloys have been the subject of a large number of publications [9]. The corrosion of aluminum alloy friction stir welds was commonly investigated using methods such as immersion tests, polarization techniques and electrochemical impedance spectroscopy (EIS) [10,11].

From the literature review, it is understood that the most of the published information on friction stir welded aluminium alloys were focused on mechanical properties. There remains a limited understanding of the corrosion properties of friction stir welded AA2024 aluminium alloys. Moreover there has not been any systematic study reporting the effect of pH values, chloride ion concentration and immersion time on the corrosion behaviour of friction stir welded AA2024 aluminium alloys. Hence, the present investigation was carried out to study the corrosion behaviour of AA2024 aluminium alloy welds. Furthermore, an empirical relationship was developed to predict the corrosion rate of friction stir welds of AA 2024 Aluminium alloy immersed in NaCl solutions.

2. Experimental Work

2.1 Fabricating the joints and preparing the specimens

The material used in this study was AA2024 aluminium alloy in the form of rolled plates of 5 mm

*Corresponding Author - E- mail: r.seetharamanme@gmail.com

thickness. The chemical composition and mechanical properties of the base metal are presented in Table 1 & 2. The optical micrograph of base metal is shown in Fig.1.

Table 1 Chemical composition (wt %) of AA2024 aluminium alloy

Mg	Mn	Fe	Si	Cu	Zn	Al
1.42	0.61	0.08	0.06	4.43	0.06	Balance

Table 2.Mechanical properties of AA2024 aluminium alloy

Material	Yield Strength (MPa)	Ultimate Tensile Strength (MPa)	Elongation (%)	Vickers Hardness (0.5 kg)
AA2024	310	402	23	140

The plate was cut to a required size (300mm x 150mm) by power hacksaw followed by milling. The square butt joint configuration was prepared to fabricate the joints. The initial joint configuration was obtained by securing the plates in position using mechanical clamps. The direction of welding was normal to the extruded direction. Single pass welding procedure was followed to fabricate the joints. A non-consumable tool made of high carbon steel was used to fabricate joints. An indigenously designed and developed computer numerical controlled friction stir welding (22kW; 4000 RPM; 60kN) was used to fabricate joints. The FSW parameters were optimized by conducting trial runs and the welding conditions which produced defect free joints were taken as optimized welding conditions. The optimized welding conditions used to fabricate the joints in this investigation are presented in Table. 3

Table 3 Optimized Welding conditions and process parameters used to fabricate the joints.

Rotational speed (rpm)	Welding speed (mm/min)	Axial force (kN)	Tool shoulder diameter (mm)	Pin diameter (mm)	Pin length (mm)
1500	75	10	15	5	4.7

The specimens were ground with 500#, 800#, 1200#, 1500# grit SiC paper. Finally, it was cleaned with acetone and washed in distilled water then dried by warm flowing air. From the welded joints, the corrosion test specimens were extracted from the friction stir welds to the dimensions of 15 mm x 15 mm x 5 mm. The optical micrograph of the friction stir weld region is shown in Fig.2.

2.2 Recording the corrosion rate

The corrosion rate of the AA2024 aluminium alloy specimen was estimated by weight loss measurement under immersion corrosion tests as per ASTM G-31. This standard practice describes the accepted procedures for and factors that influence laboratory immersion corrosion tests, particularly weight loss tests. Solutions of NaCl with concentration of 0.6M were prepared. The pH values of the solutions were maintained at pH 7.

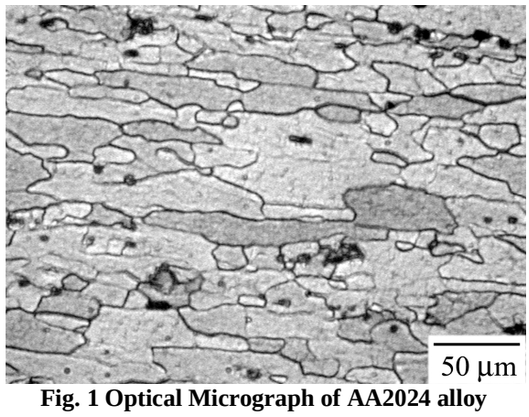

Fig. 1 Optical Micrograph of AA2024 alloy

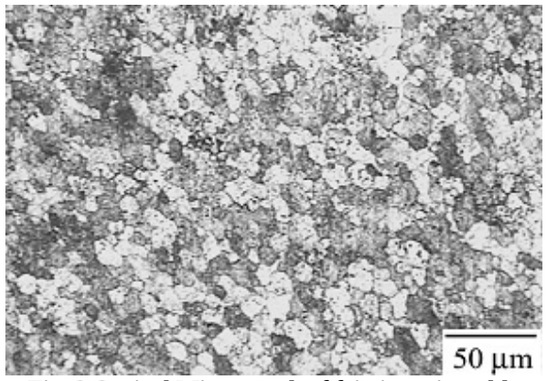

Fig. 2 Optical Micrograph of friction stir welds AA2024 alloy

The original weight (wo) of the specimen was recorded and then the specimen was immersed in the solution of NaCl for different immersion time of 24 hours, 64 hours and 104 hours Finally, the corroded products were removed by immersing the specimens for 5 to 10 minutes in a solution boiled at 90o C prepared by using 50 mL phosphoric acid (H3PO4, specific gravity of 1.69) and 20 g chromium trioxide (CrO3) Reagent water to make 1000 mL. If corrosion product films remain, rinse, and then follow with Nitric acid (HNO3, specific gravity of 1.42) for 1 to 5 min at 20 to 25°C. These

specimens were washed with distilled water, dried and weighed again to obtain the final weight (w1). The weight loss (w) could be measured using the following relation,

$$w = (w_o - w_1) \quad (1)$$

where, w = weight loss in gram, w_o = original weight before test in gram, w_1 = final weight after test in gram.

The corrosion rate of AA2024 aluminium alloy weld metal region could be calculated by using the following equation by conducting the immersion test as per ASTM standards G1-03. This standard practice suggests the procedures for preparing bare, solid metal specimens for tests, for removing corrosion products after the tests have been completed, and for evaluating the corrosion damage that has occurred. Emphasis is placed on procedures related to the evaluation of corrosion by weight loss

$$\text{Corrosion rate (mm/year)} = \frac{8.76 \times 10^4 \times w}{A \times D \times T} \quad (2)$$

Where,

w = weight loss in gram, A = surface area of the specimen in cm^2, D = density of the material, 2.73 gm/ cm^3,T = immersion time in hours

Microstructural analysis was carried on the corroded specimens using a light optical microscope (Make: Union.opt.co.ltd. Japan; Model: VERSAMET-3) incorporated with an image analyzing software (Clemex-vision). The exposed specimens surface was prepared for the micro examination both in the “AS polished” and “AS etched” conditions. Picral +Acetic acid were used as etchant. The corrosion test specimens were polished in disc polishing machine to scratch fewer surfaces and the surface was observed at 200X magnification. Furthermore, the pitting characterization and the determination of corrosion products were done using SEM-EDS.

3.0 Results & Discussion

3.1 Effect of Immersion time

With the increase of immersion time the corrosion rate decreases for the specimens undergoing immersion corrosion tests shown in Table 4. It proved that the outer layer made a predominant role to strike against corrosion with the increase of time.

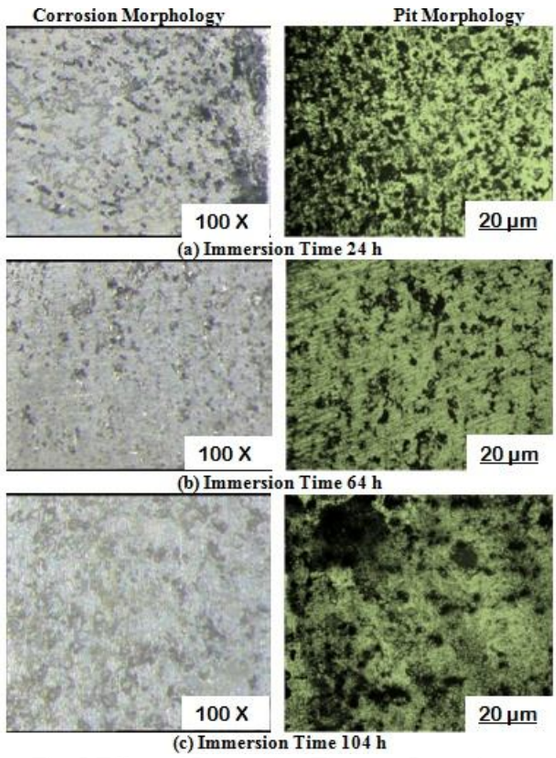

Fig. 3 Effect of Immersion Time on Corrosion morphology and Pit Morphology

Table 4 Experimental results

Experiment No.	pH value P	Immersion Time T (hours)	Chloride ion concentration C (M)	Corrosion rate CR (mm/yr)
1	7.00	24.00	0.60	0.62
2	7.00	64.00	0.60	0.49
3	7.00	104.00	0.60	0.43

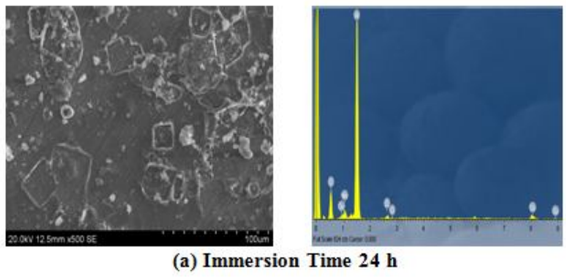

(a) Immersion Time 24 h

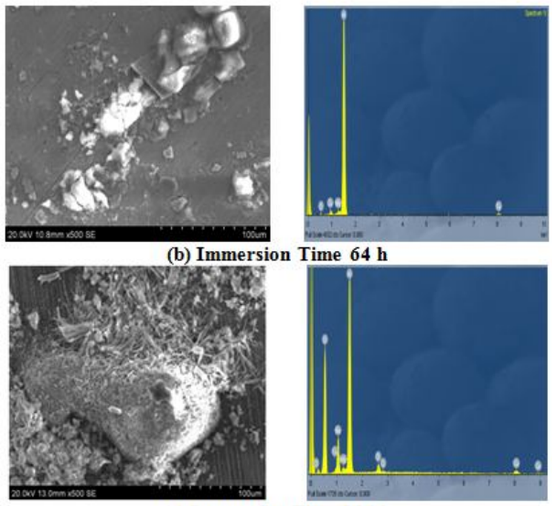

(b) Immersion Time 64 h

(c) Immersion Time 104 h

Fig. 4 SEM Analysis of AA2024 weld specimens after corrosion tests in NaCl solutions with pH 7 & Chloride ion concentration 0.6M

Fig. 3 shows the effect of immersion time on corrosion and pit morphology of AA2024 aluminium welds immersed in NaCl solutions of pH 7 with chloride ion concentration 0.6 M at different immersion time 24 h, 64 h and 104 h. During the immersion corrosion testing, dark patches were observed on the surface of the specimens with increasing exposure time. It results in an increase in hydrogen evolution with increasing exposure time, which tends to increase the concentration of OH^- ions strengthening the surface from causing further corrosion [12]. It was also found that the increase in exposure time enhanced the tendency to form corrosion products, which accumulated over the surface of the samples. However, with the increase of immersion time, the corrosion product formed is known to be $Al(OH)_3$.

From the pit morphology, the pits of very small diameter and deeper were observed on the surface after corrosion test and a continuous decrease in thickness over the entire surface area of the metal was observed throughout the corrosion test in the specimen exposed for 24 hours. But later with increment of time, the pits seems grows wider with in the presence of corrosion products. With the increase in exposure time, the depth of the corrosion pit stops increasing as the pit bottom becomes passive, but general corrosion still brushes away the top layer of the bulk material, leading to the decrease of pit depth between 64 h and 104 h. In addition, though the pit bottom becomes passive, the upper wall of pits still becomes active, allowing pits to penetrate through the underside of the corrosion film thus increasing pit area shown in the figure. In Fig. 3c a small pit on the right side coalesced with a larger pit, allowing the pit to fully open. This forms a single hemispherical-shaped corrosion pit and increases the pit area. This growth process creates some pits that are partially opened, while other pits become fully opened, inducing the large standard deviation in pit area at 104 h. The decrease in both corrosion pit area and depth at 104 h is caused by general corrosion reducing the area surrounding the pits, as well as reducing the pit depth simultaneously. Because of the large variation in the pit area and pit depth, meaning that some pits grew larger while other pits shrank. General corrosion removes the surrounding aluminium, thereby shrinking some pits and reducing their volume. The pits that increased in area and depth then averaged out the pits that decreased in area and depth, thereby leading to a pit volume that stays approximately the same throughout the experimental period. Thus with the increase of corrosion time the corrosion rate decreases.

3.2 SEM Analysis

The pitting corrosion occurred in every region after being immersed in NaCl solutions for 24 h, 64 h and 104 h with the chloride ion concentration 0.6 M and pH 7 as shown in the Fig. 4. During the early immersion of 24 h shown in Fig. 4 (a), the initial galvanic couple of pitting corrosion was founded in the region between the S phase particles and their adjacent aluminium matrix. The S phase particles as anode took priority in dissolving due to the lower self-corrosion potential compared to the adjacent aluminium matrix. Consequently, the S phase conversely acted as the cathode and led to the anodic dissolution of the adjacent aluminium matrix. Also, it was noted from the EDS, peaks of Chloride and Sodium was observed. This reveals more attack of the aluminium alloy welds since it is exposed to NaCl solutions.

For the immersion environment, however, sodium ion penetrates into the whole substrate near the pit fringe, while the chloride concentration is almost the same throughout the pit interior. In addition, the corrosion further increases because the gradient concentration is enhanced by convection in the electrolyte, making the development of a passive area difficult. The difficulty in forming a passive layer allows the sodium to migrate into the substratum surrounding the localised corrosion pit, exacerbating the corrosion attack, which makes the immersion environment more detrimental [13].

However, after 24 h had elapsed, the samples were then presenting signs of localised attack. This behaviour is similar to that described for alloy AA2024-T4. For a higher immersion period of 64 h shown in Fig. 4 (b), the corrosion attack primarily strikes the secondary phase. In this case, the grain is refined and

quite a lot of secondary phase particles are distributed along the grain boundary. The secondary phase particles cannot be easily destroyed with the increase in time because the secondary phase particles are noble to the alkaline solution. With the increase in exposure time, the quantity of the secondary phase in the exposed surface would increase and finally play the role of a corrosion barrier with the increment of time**.** From the EDS results, the corrosion products comprise the hydroxide layer which resulted from the growth of higher peak of oxygen. The hydroxide layer formed is about to stabilize with the increase in exposure time, is the dominant factor to avoid further corrosion. This is attributed to corrosion products occurring over increasing fraction of the surface, which comprises of an insoluble protective layer of $Al(OH)_3$. Thus, the corrosion rate decreases with the increase in exposure time. It shows the appearance of these intermetallics after the exposure in a solution of NaCl for 104 h. The presence of higher peaks of oxygen in the EDS and the fact that their composition hardly varies, together with the type of corrosion displayed in the neighbouring aluminium matrix, tend to confirm the cathodic character of these intermetallics. Thus the process of reduction of O_2 to OH^- takes place on these intermetallics, and the oxidation of the matrix is the associated anodic response.

The SEM images of the specimen immersed for 104 h shown in Fig. 4 (c), together with the EDS maps for Al, O, Cu, Mg, the Al maps are generally unchanged as a function of exposure time, but the area of the intermetallic becomes less well-defined as corrosion products are deposited around this site. Oxygen exhibits an interesting behaviour. After 24 h, the O signal is most intense at the periphery of the intermetallic particle, but in 104 h, the intensity is more evenly distributed over the intermetallic. Then as the exposure progresses further, the O intensity tends to be associated with the larger fragments of corrosion products which deposit on the matrix close to the intermetallic. However, at the matrix/intermetallic interface where the corrosive attack is most aggressive, the O signal is reduced [14]. Here, the O intensity increases with the increase of time leads to some corrosion inhibition. The Cl intensity is also weak, but unlike Mg increases in intensity with exposure time. The Cl is mostly concentrated on the intermetallic, but for long exposure times, Cl is also observed in the larger corrosion deposits. The local increase of the pH is also the factor responsible for the dissolution of the layer and matrix in proximity to these intermetallics. With the increase of time, the local pH of the solution increases slightly. The Cu map shows very little change during the exposure, the Cu intensity remaining intense just at the site of the intermetallic. The copper originates from the Al(Cu,Mg) intermetallics themselves; once the Al and Mg in these particles have been desalted, the remaining Cu gets dissolved due to its porous structure [15, 16]. It is this copper in solution that is then reduced on the points of cathodic character with the increase of immersion time, such as the Al intermetallics, and appears in the form of small nodules.

4.0 Conclusions

1. The corrosion rate was decreased with the increase of immersion time, but the corrosion tends to form uniform with the increase of time. With the increase in exposure time, the depth of the corrosion pit stops increasing as the pit bottom becomes passive, but general corrosion still brushes away the top layer of the bulk material, leading to the decrease of pit depth between 64 h and 104 h.

2. From the pit morphology, the pits of very small diameter and deeper were observed on the surface after corrosion test and a continuous decrease in thickness over the entire surface area of the metal was observed throughout the corrosion test in the specimen exposed for 24 hours. But later with increment of time, the pits grow wider with in the presence of corrosion products.

3. However, at the matrix/intermetallic interface where the corrosive attack is most aggressive, the O signal is reduced. Here, the O intensity increases with the increase of time leads to some corrosion inhibition

References

1. *Yi, W.S., O'grady, W.E., Ramaker, D.E. and Natishan, P.M. (2000) "Chloride ingress into aluminum prior to pitting corrosion: An investigation by XANES and XPS" Electrochemical Society, Vol 47, pp 2952-2958.*

2. *Thomas, W.M., Nicholas, E.D., Needham, J.C., Murch, M.G., Smith, P.T. and Dawes C.J. (1991) "Friction stir butt welding", International Patent Application No. PCT/GB92/ 02203, December 1991.*

3. *Thomas, W.M. and Nicholas, E.D. (1997) "Friction stir welding for the transportation industries", Materials and Design, Vol 18, pp. 269–273.*

4. *Ericsson, M. and Sandstrom, R. (2003) "Influence of welding speed on the fatigue of friction stir welds, and comparison with MIG and TIG", International Journal of Fatigue, Vol. 25, pp. 1379–1387.*

5. *Balasubramanian, V., and Lakshminarayanan, A.K.. (2008) "The mechanical properties of the GMAW, GTAW and FSW joints of the RDE-40 aluminium alloy" International Journal of Microstructure and Materials Properties, Vol. 3, pp. 837–853.*

6. *Xu, W.F., Liu, J.H., Luan, G.H. and Dong, C.L. (2009) "Microstructure and mechanical properties of friction stir welded joints of aluminum alloy thick plate with different welding state", Acta Metallurgica Sinica, Vol. 45, pp. 490–496.*

7. *Rajakumar, S., Muralidharan, C., and Balasubramanian, V. (2010) "Establishing empirical relationships to predict grain size and tensile strength of friction stir welded AA 6061-T6 aluminium alloy joints", Transactions of Non ferrous Metals Society of China, Vol. 20,pp. 1863-1872.*

8. *Díaz-Ballote, L., López-Sansores, J.F., Maldonado-López, L. and Garfias-Mesias, L.F. (2009) Electrochim. Commun. Vol. 11, pp. 41-47*

9. *Wadeson, D.A., Zhou, X., Thompson, G.E., Skeldon, P., Djapic Oosterkamp, L. and Scamans, G. (2006) Corrosion Science, Vol. 48 pp. 887 -8894.*

10. *Jariyaboon, M., Davenport, A.J., Ambat, R., Connolly, B.J., Williams, S.W. and Price, D.A. (2007), Corrosion Science Vol. 49, pp. 877-884.*

11. *Sehgal, A., Lu, D., and Frankel, G.S. (1998), Electrochemical Society, Vol. 145 pp. 28-34.*

12. *Song, W., Martin, H., Hicks, A., Seely, Christopher, D., Walton, A., Wang, P. and Horstemeyer, M.F. (2014) "Corrosion behaviour of extruded AM30 magnesium alloy under salt-spray and immersion environments" Corrosion Science, Vol. 78, pp. 353–368.*

13. *Buchheit, R.G., Grant, R.P., Hlava, P.F., Mckenzie, B. and Zender, G.L. (1997) "Local dissolution phenomena associated with S phase (Al2CuMg) particles in aluminum alloy 2024-T3", Journal of the Electrochemical Society, Vol. 144, pp. 2621–2628.*

14. *Grilli, R., Baker, M., Castle, J.E., Dunn, B. and Watts, J.F. (2010) "Localized corrosion of a 2219 aluminium alloy exposed to a 3.5% NaCl solution", Corrosion Science, Vol. 52, pp. 2855–2866.*

15. *Guillaumin, V. and Mankowski, G. (1999) "Localized corrosion of 2024 T351 aluminum alloy in chloride media", Corrosion Science, Vol. 4, pp. 421–438.*

16. *Queiroz, F.M., Magnani, M., Costa, I. and de Melo, H.G. (2008) "Investigation of the corrosion behaviour of AA2024-T3 in low concentrated chloride media" Corrosion Science, Vol. 50, pp. 2646–2657.*

